Chemical Engineering Journal 361 (2019) 528–537

Contents lists available at ScienceDirect

Chemical Engineering Journal

journal homepage: www.elsevier.com/locate/cej

Review

Study on the synthesis of poly(pyrrole methane)s with the hydroxyl in different substituent position and their selective adsorption for Pb^{2+}

Yunpeng Liu, Wenlong Zhang, Chengcheng Zhao, Hui Wang, Jie Chen, Liu Yang, Jiangtao Feng*, Wei Yan*

Department of Environmental Science & Engineering, State Key Laboratory of Multiphase Flow in Power Engineering, Xi'an Jiaotong University, Xi'an 710049, China

HIGHLIGHTS

- Poly(pyrrole methane)s differing in substituent positions of –OH were synthesized.
- Poly(pyrrole methane)s exhibit excellent selective adsorption for Pb^{2+}.
- Different Pb^{2+} adsorptions on poly (pyrrole methane)s result from steric hindrance.
- The influence of other metal ions on Pb^{2+} adsorption was supported by HSAB theory.

GRAPHICAL ABSTRACT

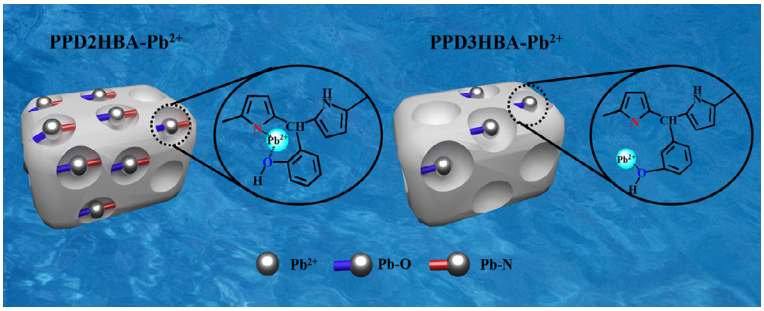

ARTICLE INFO

Keywords:
Poly(pyrrole methane)
Steric hindrance
HASB theory
Selective adsorption
Heavy metal ions

ABSTRACT

Two poly(pyrrole methane)s (PPD2HBA and PPD3HBA) were successfully synthesized, with focusing on the effect of steric hindrance on the selective adsorption of heavy metal ions. The structure and morphology of PPD2HBA and PPD3HBA were characterized by FT-IR, UV–Vis, ^{1}H NMR, BET, SEM, XPS and Zeta potential. The influencing factors of the Pb^{2+}-adsorption onto the two adsorbents were systematically studied, including various solution conditions and co-existing metal ions effect. These results demonstrated that the two adsorbents showed slightly different adsorption behaviors. The maximum adsorption capacities of Pb^{2+} onto PPD2HBA and PPD3HBA were 41.35 and 32.10 mg·g^{-1} at pH = 6.0 and 318 K, respectively. The crucial steric hindrance verified by FT-IR and XPS before and after Pb^{2+} adsorption, showed better consistence in PPD2HBA with the size and shape of the hydrated Pb^{2+} than that in PPD3HBA, which can be further supported by the adsorption property of PPD4HBA. In addition, the effect of the co-existing metal ions of Pb^{2+} onto PPD2HBA and PPD3HBA could be testified by the HSBA theory. The proposed adsorption mechanism in this paper was of remarkable potential for the design of new adsorbent to selectively adsorb heavy metal ions from wastewater.

1. Introduction

Heavy metal pollution in wastewater has become a worldwide environmental concern, with its high toxicity to biological system even with trace amount [1]. Many methods have been commonly used to removal the heavy metal ions from industrial effluents, including chemical precipitation, ion exchange, membrane filtration, adsorption, etc [2–4]. Among these methods, adsorption is generally regarded as the most effective technology with advantages of low cost and simple process [5,6].

* Corresponding authors.
E-mail addresses: fjtes@xjtu.edu.cn (J. Feng), yanwei@xjtu.edu.cn (W. Yan).

https://doi.org/10.1016/j.cej.2018.12.093
Received 10 October 2018; Received in revised form 16 December 2018; Accepted 18 December 2018
Available online 19 December 2018
1385-8947/

Recently, more and more materials were employed as adsorbent to removal heavy metal ions, including mainly zeolite [7], clay [8], polymer [9] and activated carbon [10]. However, many researchers paid attention to the adsorption capacity, but not the selectivity adsorption to different heavy metal ions. What is more, as a kind of important and non-renewable resource, heavy metals have high market value and strategic significance. Therefore, developing the selectivity of adsorbents to different heavy metals is of long-term prospects.

Nowadays, selective adsorption of heavy metal ions mainly includes two main mechanisms: Firstly, when the adsorbent modified with specific functional groups (–NH_2, –COOH, –SH, etc.), some or certain types of heavy metal ions could be preferentially adsorbed through complexation or chelation interaction according to the hard and soft acids and bases theory (HSAB) [11,12]. Wang et al. [13] used the aqueous sodium alginate solution for direct gelation with metal ion. –COO^- and –OH groups on alginates exhibited higher affinities toward Pb^{2+} than Cu^{2+} and Cd^{2+}. Cui et al. [14] synthesized the magnetic graphene oxide with EDTA functionalized to adsorb Pb^{2+}, and FT-IR analysis indicated that both –COOH and –OH groups were involved in the binding process with Pb^{2+}; Secondly, based on the ion imprinting technology, the polymerization of functional monomers can use specific metal ions as templates. Then, after removing the template ions, the well-order functional groups and the cavity with fixed size and shape show excellent selective adsorption for metal ions [15,16]. Ge et al. [17] designed the glutaraldehyde-crosslinked chitosan with acrylic acid grafted by using Pb^{2+} as template, and this adsorbent had good selective adsorption capacity for Pb^{2+}. Esen et al. [18] prepared the material which used N-methacryloyl-(L)-cysteine as functional monomer and Pb^{2+} as template, and this adsorbent had good ions recognition of Pb^{2+} for well steric hindrance. However, the ion imprinting technology has to remove the template ions by using acid liquor, which will raise the cost of the adsorbent and bring further pollutions. Hence, it could be possible to prepare new adsorbent combined the ion imprinting technology and the affinity between metal ions and functional groups, thus can inhabit the defect of ion imprinting technology.

Poly(pyrrole methane), similar to ring-opening porphyrin, is a kind of π-conjugated polymer which is synthesized with pyrrole and aldehyde in acidic conditions [19]. Poly(pyrrole methane) is the precursor of poly(pyrrole methine), therefore, it has been paid great attention in many fields including photoluminescence, photovoltaic cell, optical nonlinearity, etc [20–22]. Meanwhile it's expected to be used as a new blue luminescent material due to its blue fluorescent property [23,24]. The chemical structure of poly(pyrrole methane) can be different adjustable by changing the type of aldehyde. When aromatic aldehyde with functional groups is used to synthesize the poly(pyrrole methane), the steric hindrance, namely the interspace between functional groups and imine of pyrrole ring, could be formed. Hence, the poly(pyrrole methane) with different steric hindrance could be synthesized to selectively adsorb metal ions. So far, the adsorption capability especially the selective adsorption of poly(pyrrole methane) is rarely reported in the literatures. Therefore, the selective removal of heavy metal ions by poly(pyrrole methane) is of great potential.

In this study, we fabricated two poly(pyrrole methane)s, poly[pyrrole-2, 5-diyl (2-hydroxybenzylidane)] (PPD2HBA) and poly[pyrrole-2, 5-diyl (3-hydroxybenzylidane)] (PPD3HBA), and their selective adsorption behaviors were also systematically studied. Through changing the substituent position of hydroxyl in benzene ring, we attempted to provide the theory of the relationship between the selective adsorption of metal ions and the steric hindrance.

2. Materials and methods

2.1. Chemicals

Pyrrole (98%, Sinopharm Chemical Reagent Co., Ltd, Shanghai, China) was freshly distilled, and then stored under the aerated nitrogen condition in a refrigerator (0 °C) before used. Analytical grade reagents of 3-hydroxybenzaldehyde, 2-hydroxybenzaldehyde, dimethyl sulfoxide (DMSO), tetrahydrofuran (THF), n-hexane , $PbCl_2$, $CdCl_2$ and $NiCl_2$were also purchased from Sinopharm Chemical Reagent Co., Ltd, (Shanghai, China). All other chemicals were of analytical grade without further purification and distilled water was used in the preparation of all solutions.

2.2. Synthesis of two poly(pyrrole methane)s

The two poly(pyrrole methane)s were synthesized by copolymerizing pyrrole and corresponding aromatic aldehydes in acidic conditions. In a typical experiment, 1.0 mmol aromatic aldehyde was dissolved into the 50 mL DMSO solution containing 9.70 mL HCl under N_2 atmosphere. And 50 mL DMSO solution including 1.0 mmol pyrrole monomer was dropped slowly in above solution, and stirred for 24 h at room temperature. After that, the mixture solution was continued to react under vacuum atmosphere at 60 °C for another 2 h. Then, the mixture was poured into 2 mol·L^{-1} ammonia solution. The deposited solid was alternatively centrifuged and washed with deionized water until pH reached neutral. The above solid was dissolved into 100 mL THF, and then the mixture was poured into the 1000 mL n-hexane. Finally, the deposited matter was filtrated and washed with deionized water to remove residual DMSO solution, and dried overnight in vacuum drying oven at 50 °C; The sample composited of 2-hydroxybenzaldehyde was named as PPD2HBA. ^{1}H NMR (500 MHz, DMSO-d_6, δ): 9.46–9.00 (broad, 1H, NH), 7.57–6.41 (m, 6H, Pyr-H Ar-H and OH), 5.31 (s, 1H, $(Pyr)_2$-CH-Ar) (Fig. S1a); The 3-hydroxybenzaldehyde was for PPD3HBA. ^{1}H NMR (500 MHz, DMSO-d_6, δ): 9.35–8.98 (broad, 1H, NH), 7.68–6.28 (m, 6H, Pyr-H Ar-H and OH), 5.47 (s, 1H, $(Pyr)_2$-CH-Ar) (Fig. S1b) [24]. The synthetic reaction to PPD2HBA and PPD3HBA were outlined in reaction (1) and (2), respectively.

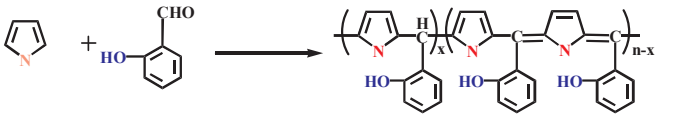

(1)

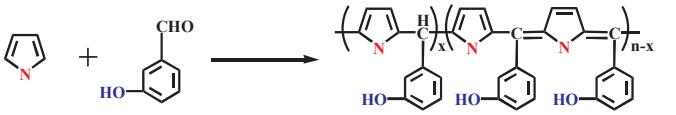

(2)

2.3. Characterizations

The flourier transformation infrared spectroscopy (FT-IR) spectrums of samples were recorded on a Bruker TENSOR 37 FT-IR spectrophotometer in the region from 400 to 4000 cm^{-1} by the KBr pellet method. The X-ray photoelectron spectroscopy (XPS) spectrums of samples were performed on Thermo Scientific EscaLab 250Xi with an Al monochromatic X-ray source (1486.6 eV), and all binding energies (BEs) were referenced to the C 1 s hydrocarbon peak at 284.8 eV. The morphology of samples were investigated by scanning electron microscope (SEM Zeiss Gemini SEM 500). The Barrett-Emmett-Teller specific surface area (S_{BET}), total pore volume (V), and average pore radius (R) were performed by the Builder SSA-4200 (Beijing, China) at 77 K using the Barrett-Joyner-Halenda (BJH) method. The chemical structural formulas of samples were confirmed by the ^{1}H NMR spectrum (Bruker III HD 400 M) and UV–vis absorption spectrum (Agilent 8453). The Zeta potentials of the samples were measured by Nanobrook-Omni, through adding 3 mg sample in 10 mL NaCl solution (10^{-3} mol·L^{-1}) with different pH values (pH = 1–12, adjusted by 0.1 mol·L^{-1} HNO_3 or NaOH solution).

2.4. Adsorption experiments

All adsorption experiments were placed into centrifuge tubes which contained 40 mg absorbent and 20 mL 100 mg·g^{-1} Pb^{2+} solutions at pH 6, and were fixed in the temperature controlled shaker with the agitation of 220 rpm for 24 h at 298 K. After that, the mixture were filtered with 0.22-μm membrane. The concentrations of heavy metal ions in the original and such collected solutions were measured by inductively coupled plasma emission spectrometer (ICPE-9000, Japan). The adsorption capacity (mg·g^{-1}) of metal ions onto the sample was calculated according to the formula (1) as follow:

$$q_e = \frac{(C_0 - C_e)V}{m} \tag{1}$$

where q_e is the equilibrium adsorption capacity of the adsorbent (mg·g^{-1}), C_0 (mg·L^{-1}) and C_e (mg·L^{-1}) are initial and equilibrium concentration of metal ions, respectively. V (L) is the solution volume, and m (g) is the weight of adsorbent used.

To study the effect of solution pH values, the solution pH values were adjusted ranging from 1 to 6 (regulating with 0.1 mol·L^{-1} HCl/NaOH); The equilibrium isotherm studies were conducted with Pb^{2+} solutions ranging from 50 to 600 mg·g^{-1} at 298, 308 and 318 K, respectively; In the adsorption kinetics studies, the suspension which derived in three kinds of Pb^{2+} solutions (50, 100 and 150 mg·g^{-1}), was sampled at regular intervals; In order to study the effect of co-existing metal ions, the binary solutions which contained 100 mg·L^{-1} Pb^{2+} and 100 mg·L^{-1} other cation (Cd^{2+} and Ni^{2+}) were employed. Meanwhile, according to the data of competitive adsorption in binary solution, the selectivity of the two adsorbents for Pb^{2+} were evaluated by the selectivity coefficient ($\beta_{Pb^{2+}/M^{n+}}$), and comparing with other metal ions (Cd^{2+} and Ni^{2+}). The higher the β value shows better the selective adsorption performance of the adsorbent. The selectivity coefficient is defined as formula (2) [25]:

$$\beta_{Pb^{2+}/M^{n+}} = \frac{D_{Pb^{2+}}}{D_{M^{n+}}} \tag{2}$$

where $D_{Pb^{2+}}$ and $D_{M^{n+}}$ are distribution ratios of Pb^{2+} and other co-existent metal ions in mixed solution, respectively. The distribution ratio (D) was calculated by formula (3):

$$D = \frac{C_0 - C_e}{C_0} \times \frac{V}{m} \tag{3}$$

where C_0 (mg·L^{-1}) and C_e (mg·L^{-1}) are initial and equilibrium concentration of metal ions, respectively. V (L) is the solution volume, and m (g) is the weight of adsorbent used.

In order to testify the relationship between the selectivity adsorption of metal ions and the different steric hindrances, poly[pyrrole-2, 5-diyl (4-Hydroxybenzylidane)] (PPD4HBA) was also synthesized by using same method with PPD2HBA and PPD3HBA, and was carried in adsorption experiments.

3. Results and discussions

3.1. Structural characterization of the as-prepared samples

The FT-IR spectra of PPD2HBA and PPD3HBA are shown in Fig. 1. The major characteristic bands of PPD2HBA could be assigned as follows: 3405 cm^{-1} (N–H stretch of pyrrole ring), 3217 cm^{-1} (–OH stretch of benzene ring), 2820 cm^{-1} (C–H stretch of backbone), 1696 cm^{-1} (C=C stretch of quinoid pyrrole ring), 1595 cm^{-1} (C=C stretch of benzene ring), 760 cm^{-1} (C–H out-of-plane blend of the a-linkage in pyrrole ring) [26–28]. For PPD3HBA, its FT-IR spectrum is almost similar to PPD2HBA, which is slightly different in 1750–1950 cm^{-1} due to the different substituent position of –OH. These peaks of the two poly (pyrrole methane)s indicate that the pyrrole are polymerized successfully with corresponding aromatic aldehyde in this work.

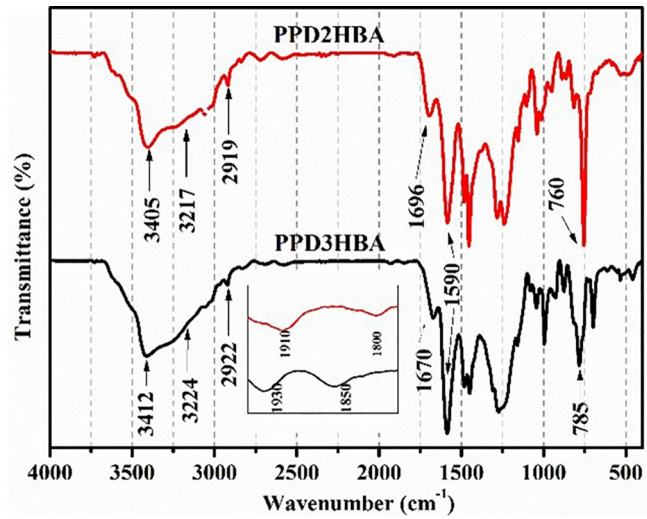

Fig. 1. FTIR spectra of PPD2HBA and PPD3HBA.

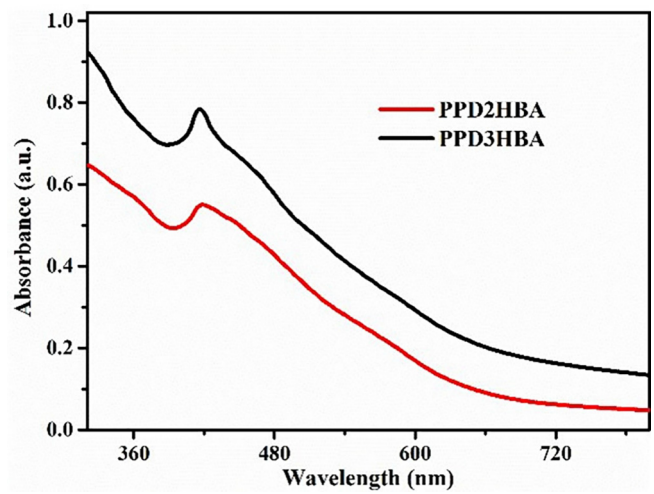

Fig. 2. UV–Vis absorption spectra of PPD2HBA and PPD3HBA.

The UV–Vis absorption spectra of PPD2HBA and PPD3HBA are depicted in Fig. 2. It is found that PPD2HBA and PPD3HBA have significant optical absorptions in the visible light range of 400–450 nm with obvious adsorption peaks at 416 and 410 nm, respectively. As the existence to the π-π* transition of the π-conjugated electron of poly (pyrrole methane) [19], it confirmed that the incomplete p-conjugated backbone of them [29]. This result also proved their molecular formula.

SEM images of PPD2HBA and PPD3HBA are shown in Fig. 3. It is obvious that both of them are coralloid-like aggregate with porous surface. PPD2HBA has more flourishing pores compared with that of PPD3HBA. The textural properties of the samples are listed in Table 1. It can be seen that the S_{BET} and V of PPD2HBA could attain 70.42 m^2·g^{-1} and 0.062 cm^3·g^{-1} (Fig. S2a), which are more than that of PPD3HBA (49.11 m^2·g^{-1}, 0.046 cm^3·g^{-1}) (Fig. S2b). This result could also back up the observation of SEM images.

Considering the important electrostatic attraction effect between the adsorbents and ions, the surface potential values of the adsorbent at different pH act as important factor to reflect the adsorption properties [30]. According to Fig. 4, it is observed that the potentials of PPD2HBA and PPD3HBA decrease with the increase of the solution pH, and pH_{zpc} of them is about 3.98 and 4.36, respectively. When the solution pH is below the pH_{zpc}, the negatively charged poly(pyrrole methane)s can greatly attract positive metal cations. While similarly at pH above their pH_{zpc}, the generated electrostatic repulsion will decrease the adsorption

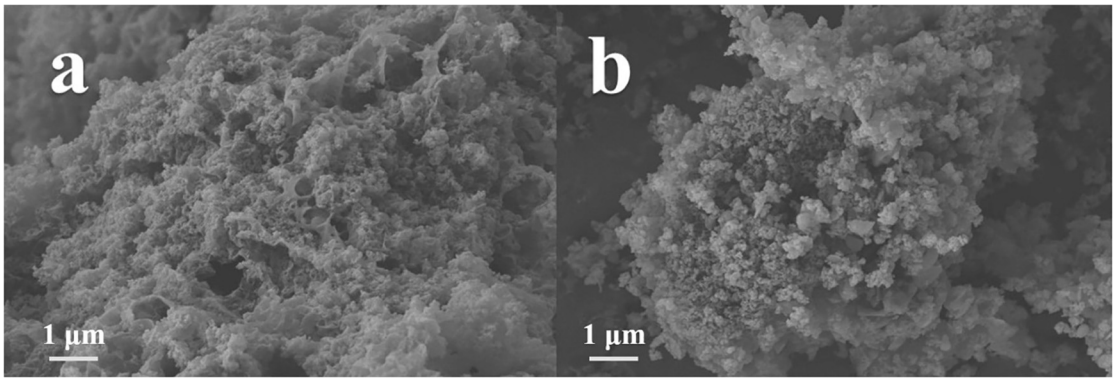

Fig. 3. SEM images of PPD2HBA (a) and PPD3HBA (b).

Table 1
Tissure properties of PPD2HBA and PPD3HBA.

Sample	S_{BET} ($m^2 \cdot g^{-1}$)	V ($cm^3 \cdot g^{-1}$)	R (nm)
PPD2HBA	70.42	0.62	17.8
PPD3HBA	49.11	0.46	18.8

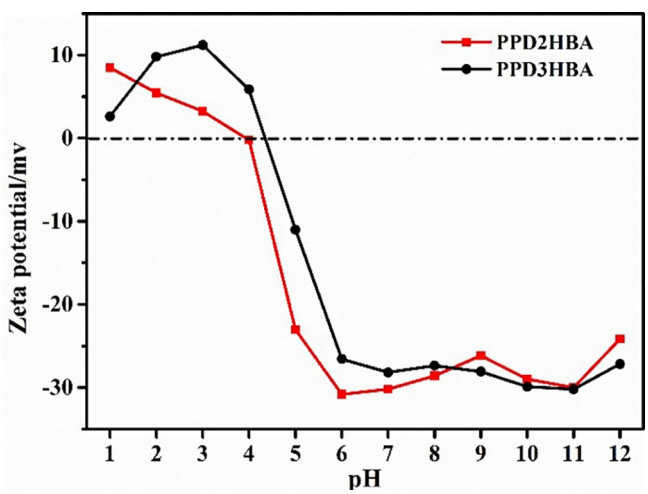

Fig. 4. Zeta potentials of the samples.

capacity.

3.2. Adsorption of the two poly(pyrrole methane)s for Pb^{2+} ions

3.2.1. Effect of pH

Fig. 5 exhibits the effect of initial pH value of Pb^{2+} solution on the adsorption capacity of the two poly(pyrrole methane)s. It can be observed that the adsorption capacities of the two adsorbents are positively affected by the solution pH, and increased with pH increasing from 2 to 6. The maximum adsorption capacities of PPD2HBA and PPD3HBA for Pb^{2+} are 29.1 and 24.9 $mg \cdot g^{-1}$ at pH 6, respectively. Combining the results of Zeta potentials, it is because the two adsorbents have both the imine of pyrrole ring and hydroxyl of benzene ring. When the solution pH is at low value, the low adsorption capacity of Pb^{2+} can be attributed to the fact that the surfaces of the two adsorbents become highly protonated and positively changed. A similar effect of pH on the polymer adsorbents is also observed [31,32]. Meanwhile, with the increase of the solution pH, the protonation of functional groups and its resulted electrostatic repulsion weakened, while the concentration of OH^- around the adsorbent increase, which promotes the chelation between metal ions and adsorbents. Therefore,

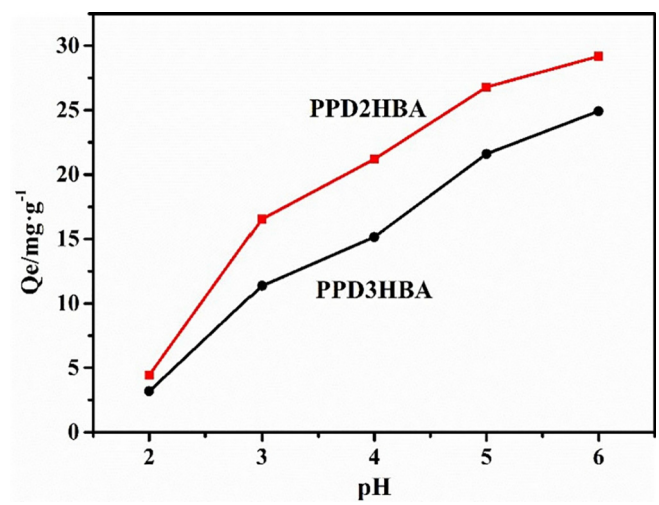

Fig. 5. Effect of solution pH on the adsorption capacity of Pb^{2+} onto the two adsorbents.

the optimal pH is chosen at pH 6 in the following experiments, with another note for avoiding the sediment of Pb^{2+} at higher pH.

3.2.2. Adsorption kinetics

The influence of the contact time for adsorption capacity of Pb^{2+} onto PPD2HBA and PPD3HBA with different initial concentrations (50, 100, 150 $mg \cdot L^{-1}$) are shown in Fig. 6. Evidently, a fast adsorption of Pb^{2+} is observed onto the adsorbents during the first 50 min, and gradually reaches the adsorption equilibrium after 150 min at three Pb^{2+} solution concentration. The initial adsorption rate of PPD2HBA is higher than that of PPD3HBA, which could be ascribed to the better affinity between PPD2HBA and Pb^{2+} due to the different substituent positions of the hydroxide groups.

The adsorption kinetics of Pb^{2+} onto the two adsorbents are analyzed under two kinetic models, namely pseudo-first-order (4) and pseudo-second-order models (5), respectively [14,33]. The two kinetics models are used in Fig. 6.

$$Q_t = Q_e(1 - e^{-k_1 t}) \tag{4}$$

$$Q_t = \frac{k_2 Q_e^2 t}{1 + k_2 Q_e t} \tag{5}$$

where k_1 (min^{-1}) and k_2 ($g \cdot mg^{-1} \cdot min^{-1}$) are successively the rate constants for the pseudo-first-order and pseudo-second-order; Q_t ($mg \cdot g^{-1}$) is the amount adsorbed at time t (min), and Q_e ($mg \cdot g^{-1}$) is the equilibrium adsorption capacity.

The relevant parameters of the two kinetics are calculated and listed in Table 2. It can be observed that the correlation coefficients of the

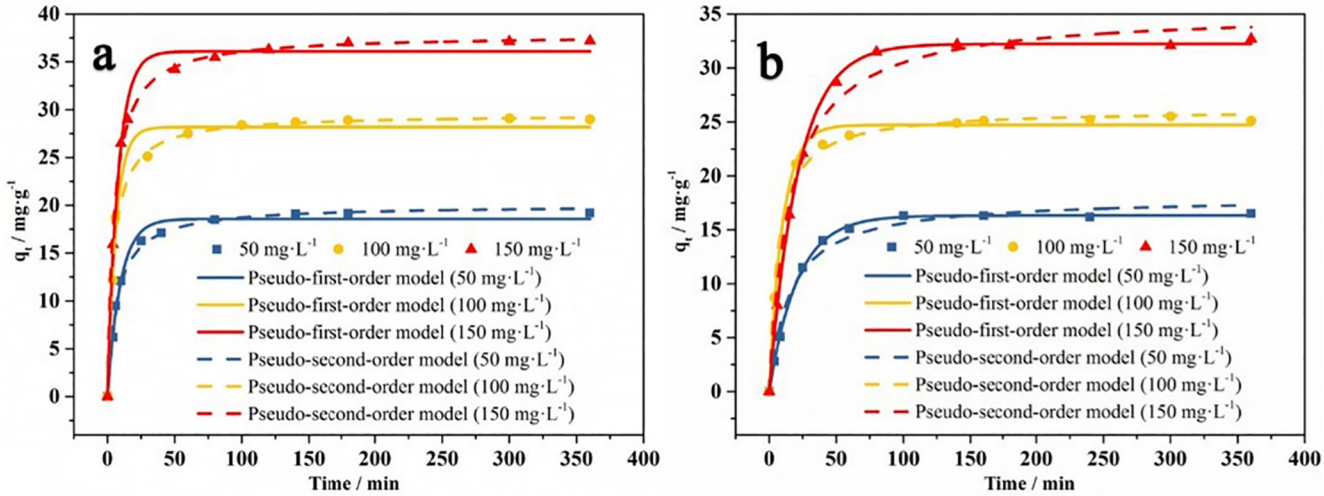

Fig. 6. Adsorption kinetics plots of Pb^{2+} onto PPD2HBA (a) and PPD3HBA (b) at different initial concentrations.

pseudo-first-order model (R^2 = 0.9933–0.9994) are more appropriate to describe the adsorption kinetics of PPD3HBA for Pb^{2+} than the pseudo-second-order model (R^2 = 0.9836–0.9930). However, for the adsorption kinetics of PPD3HBA for Pb^{2+}, the correlation coefficients of the pseudo-second-order model (R^2 = 0.9908–0.9997) are higher than the pseudo-first-order model (R^2 = 0.9817–0.9895). Moreover, the values of q_e calculated from the adsorption kinetics model whose R^2 is relatively high, agreed well with the experimental consequences. Therefore, these data show the adsorption of Pb^{2+} onto PPD2HBA preferably followed the pseudo-second-order model, which indicates that the adsorption process of Pb^{2+} onto PPD2HBA is mainly monolayer and chemical adsorption. Nonetheless, the adsorption of Pb^{2+} with PPD3HBA is agreed well with pseudo-first-order model, which indicates that the adsorption process of Pb^{2+} onto PPD2HBA appears to be controlled by the diffusion process [27,31]. The difference of adsorption processes between PPD2HBA and PPD3HBA could be generated from different positions of the hydroxide groups.

3.2.3. Adsorption isotherm

Adsorption isotherm is critical in optimizing the use of adsorbent, because it can be used to not only evaluate the adsorption capacities of adsorbents, but also describe the interaction between adsorbates and adsorbents. There are two typical adsorption isotherm models, Langmuir (6) and Freundlich (7) isotherms, to be used to analyze the equilibrium data. Their non-linear formula are expressed as follows [34]:

$$q_e = \frac{q_{\max} K_L C_e}{1 + K_L C_e} \tag{6}$$

$$q_e = K_f C_e^{1/n} \tag{7}$$

where C_e (mol·L^{-1}) is the equilibrium concentration of adsorbate; q_e (mg·g^{-1}) is equilibrium adsorption capacity and q_{max} is the maximum adsorption capacity (mg·g^{-1}); K_L (L·mol^{-1}) is the Langmuir constant which is related to the affinity of adsorbate and the binding sites; K_f (L·mg^{-1})$^{1/n}$ is the Freundlich constant indicated the relative adsorption capacity of the adsorbent; n is constant representing the adsorption intensity.

Pb^{2+} adsorption equilibrium isotherms onto the PPD2HBA and PPD3HBA at different temperatures are depicted in Fig. 7, and the relevant parameters and the correlation coefficient (R^2) are shown in Table 3. It can be seen that the adsorption isotherms are agreed better with the Langmuir model than the Freundlich model for adsorption of Pb^{2+} onto the two adsorbents at different temperatures, which indicates that their adsorption process is a monolayer adsorption [35,36]. The maximum adsorption capacity (q_{max}) of Pb^{2+} onto PPD2HBA and PPD3HBA are 41.35 and 32.10 mg·g^{-1} at 318 K, respectively. Obviously, for the two adsorbents with similar chemical structures, the difference in the substituent positions of hydroxy groups cause a discrepancy in the maximum adsorption capacity of Pb^{2+} between the two adsorbents.

Meanwhile, a dimensionless constant (R_L), which is used to find out the applicability of Langmuir model, is expressed in the following equations [37]:

$$R_L = \frac{1}{1 + K_L C_0} \tag{8}$$

where, C_O is the initial concentration of Pb^{2+}, and K_L is Langmuir constant. The value of R_L indicates irreversible equilibrium when $R_L = 0$, favorable equilibrium when $0 < R_L < 1$, linear case when $R_L = 1$ or unfavorable equilibrium when $R_L > 1$ [38]. According to the experimental data, the values of R_L are calculated as 0.005, 0.008 and

Table 2
Parameters of kinetics models for Pb^{2+} onto PPD2HBA and PPD3HBA.

Sample	C_o /mg·L^{-1}	Pseudo first order model			Pseudo second order model		
		k_1 /1·min^{-1}	q_e /mg·g^{-1}	R^2	k_2 /g·min·mg^{-1}	q_e /mg·g^{-1}	R^2
PPD2HBA	50	0.105	18.57	0.9886	0.008	19.87	0.9908
	100	0.159	28.18	0.9817	0.007	29.54	0.9912
	150	0.129	36.10	0.9895	0.005	37.84	0.9977
PPD3HBA	50	0.047	16.33	0.9994	0.003	18.01	0.9836
	100	0.099	24.72	0.9933	0.006	26.16	0.9930
	150	0.047	32.34	0.9975	0.002	35.26	0.9864

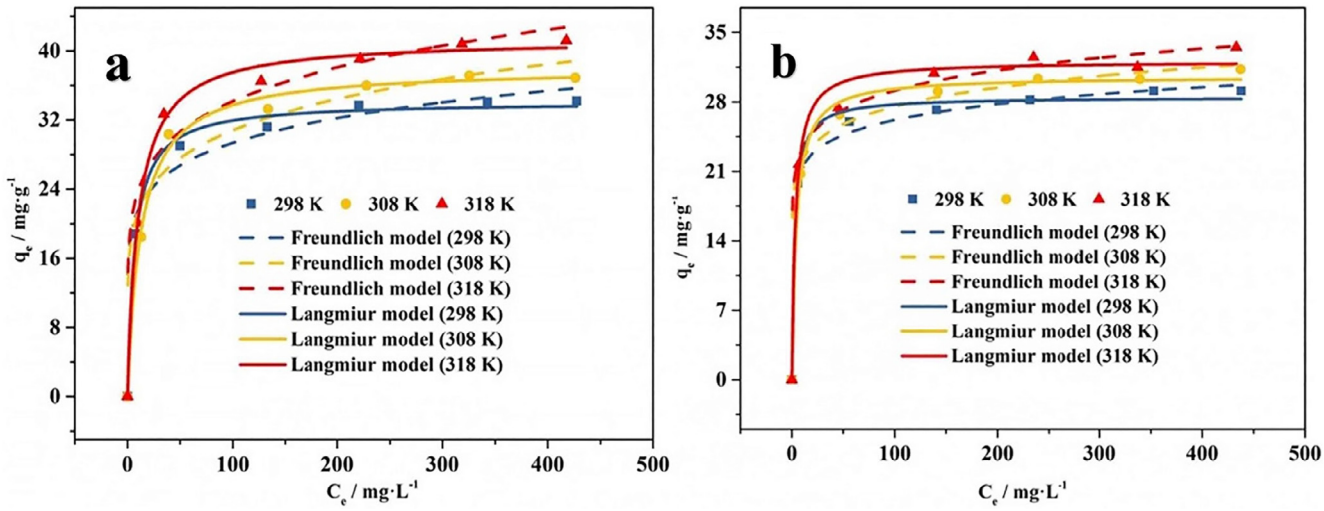

Fig. 7. Adsorption isotherm for the adsorption of Pb^{2+} onto PPD2HBA (a) and PPD3HBA (b).

Table 3
Isotherms parameters for the adsorption of Pb^{2+} onto PPD2HBA and PPD3HBA.

Sample	Temperature (K)	Langmuir isotherm				Freundlich isotherm		
		q_{max} /mg·g^{-1}	K_L /L·mg^{-1}	R^2	R_L	K_F /(mg/g)/(L/mg)	n	R^2
PPD2HBA	298	34.12	0.1461	0.9949	0.014	15.80	7.4382	0.9041
	308	38.02	0.0784	0.9939	0.025	14.76	6.2578	0.8302
	318	41.35	0.0979	0.9954	0.020	16.59	6.3686	0.8779
PPD3HBA	298	28.48	0.3713	0.9902	0.005	17.62	11.6333	0.9561
	308	30.55	0.2329	0.9945	0.008	17.68	10.3906	0.9462
	318	32.10	0.2856	0.9958	0.007	18.57	10.2207	0.9519

Table 4
Thermodynamic parameters for the adsorption of Pb^{2+} onto two adsorbents.

Sample	ΔH/kJ·mol^{-1}	ΔS/J·K^{-1}·mol^{-1}	ΔG/kJ·mol^{-1}	
PPD2HBA	19.09	59.074	25 °C	−17.585
			35 °C	−18.175
			45 °C	−18.766
PPD3HBA	10.57	29.281	25 °C	−8.715
			35 °C	−9.008
			45 °C	−9.301

0.007 at the temperature of 293 K, 303 K, 318 K for PPD3HBA, respectively. Meanwhile, the values of R_L are calculated as 0.014, 0.025 and 0.020 at 293 K, 303 K, 318 K for PPD2HBA, respectively. These dates suggest the adsorption process is favorable at operated conditions.

3.2.4. Thermodynamics study

The values of thermodynamic parameters, including the Gibb's free energy change (ΔG), enthalpy change (ΔH) and entropy change (ΔS), can be calculated from the following Eqs. (9) and (10) [39,40]:

$$\Delta G = -RT \ln K_L \tag{9}$$

$$\ln K = \frac{\Delta S}{R} - \frac{\Delta H}{RT} \tag{10}$$

where ΔG (kJ·mol^{-1}) is the Gibb's free energy change of adsorption, K_L is the Langmuir constant, R (8.314 J·mol^{-1}·K^{-1}) is the universal gas constant, T is the temperature in K, ΔS is entropy change (J·mol^{-1}·K^{-1}) and ΔH is the enthalpy change (kJ·mol^{-1}). The ΔH and ΔS values can be calculated from the slope and intercept of a linear plot of ln$K$ versus 1/T. The obtained values of ΔG, ΔH and ΔS which indicate the adsorption

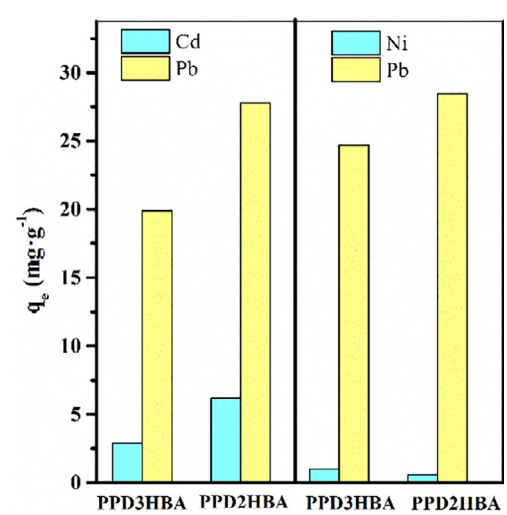

Fig. 8. Adsorption capacity of Ni^{2+}, Cd^{2+} and Pb^{2+} from binary mixtures (each metal concentration: 100 mg/L, adsorbents: 2 g/L, temperature: 25 °C, pH: 6 and contact time: 2 h).

of Pb^{2+} onto PPD2HBA and PPD3HBA under different temperatures are listed in Table 4.

The positive values of ΔH confirm the endothermic nature of adsorption process of Pb^{2+} onto the two adsorbents. The positive values of ΔS reveal that the possibility of increasing randomness at the solid liquid interface occurs in the adsorption of Pb^{2+} onto the two adsorbents. The negative values of ΔG indicate that their adsorptions are the spontaneous and feasible process. Furthermore, the values of ΔG of

Table 5
Adsorption Selectivity coefficient of some adsorbents for Pb(II) adsorption.

Adsorbent	Selectivity coefficient $\beta_{Pb/Cd}^{2+2+}$	Selectivity coefficient $\beta_{Pb/Ni}^{2+2+}$	Ref.
Ion imprinting material (Pb–ITMCB)	3.62	3.00	[43]
Xanthate-modified chitosan	2.1	2.57	[44]
Poly ethylene oxide (PEO)/Chitosan nanofiber membrane	0.93	0.64	[45]
Shells of hazelnut	1.72	2.13	[46]
Egyptian Na-activated bentonite	1.78	2.04	[47]
Nano-zirconium silicate	0.71	1.32	[48]
Sodium trititanate whisker/chitosan polymer	3.77	12.25	[49]
PPD2HBA	4.48	47.41	This work
PPD3HBA	6.86	24.70	This work

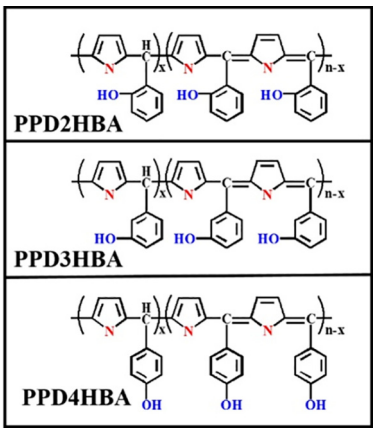

Fig. 9. The chemical structure of the three ploy(pyrrole methane)s.

Table 6
Adsorption capacity of Pb^{2+} onto three kinds of adsorbents (the concentration of Pb^{2+}: 100 mg·L^{-1}, adsorbents: 2 g·L^{-1}, temperature: 25 °C, pH: 6 and contact time: 24 h).

Sample	q_e/mg·g^{-1}
PPD2HBA	29.1
PPD3HBA	24.9
PPD4HBA	24.4

the two adsorbents are becoming more and more negative with the increase of temperature, which suggest that the higher temperature may facilitate the adsorption of Pb^{2+} onto PPD2HBA and PPD3HBA.

3.3. Mechanism of the Pb^{2+} adsorption onto the as-prepared adsorbents

3.3.1. Effect of the co-existing metal ions on Pb^{2+} adsorption

The presence of the other metal ions in aqueous solution could affect the adsorption capacity of Pb^{2+} onto the adsorbents. Therefore, it's necessary to investigate the influence of coexisting ions (Cd^{2+} and Ni^{2+}) during the adsorption process of Pb^{2+}. As shown in Fig. 8, all of coexisting ions have no significant competitive influence on the adsorption of Pb^{2+} onto the PPD2HBA and PPD3HBA. The results show better affinity of the two adsorbents with Pb^{2+} than the other two heavy metal ions, and it can be supposed that the combination strength between the two adsorbents and heavy metal ions are different. According to HSAB theory, Pb^{2+} is categorized as the intermediate acid while Cd^{2+} and Ni^{2+} is regarded as soft acid. On the other hand, the –OH and –NH- in the two adsorbents can be considered as the hard base [12,41]. Generally, hard base prefers to bond with hard acid while soft base with soft acid, and intermediate acid can bond with hard base and soft base [42]. Hence, the affinity between Pb^{2+} and –OH/–NH- of the two adsorbents are stronger than that of the other metal ions. This result demonstrates the selective adsorption of heavy metal ions are controlled by HASB theory to a certain extend. Meanwhile, in order to compare with the selective adsorption capacity of other common material, the selectivity coefficient ($\beta_{Pb/Cd}^{2+2+}$ and $\beta_{Pb/Ni}^{2+2+}$) of the two adsorbents are also calculated (Table 5). The $\beta_{Pb/Cd}^{2+2+}$ and $\beta_{Pb/Ni}^{2+2+}$ for PPD2HBA are 4.48 and 47.41, respectively. As to PPD3HBA, the selective coefficient of $\beta_{Pb/Cd}^{2+2+}$ and $\beta_{Pb/Ni}^{2+2+}$ are 6.68 and 24.70,

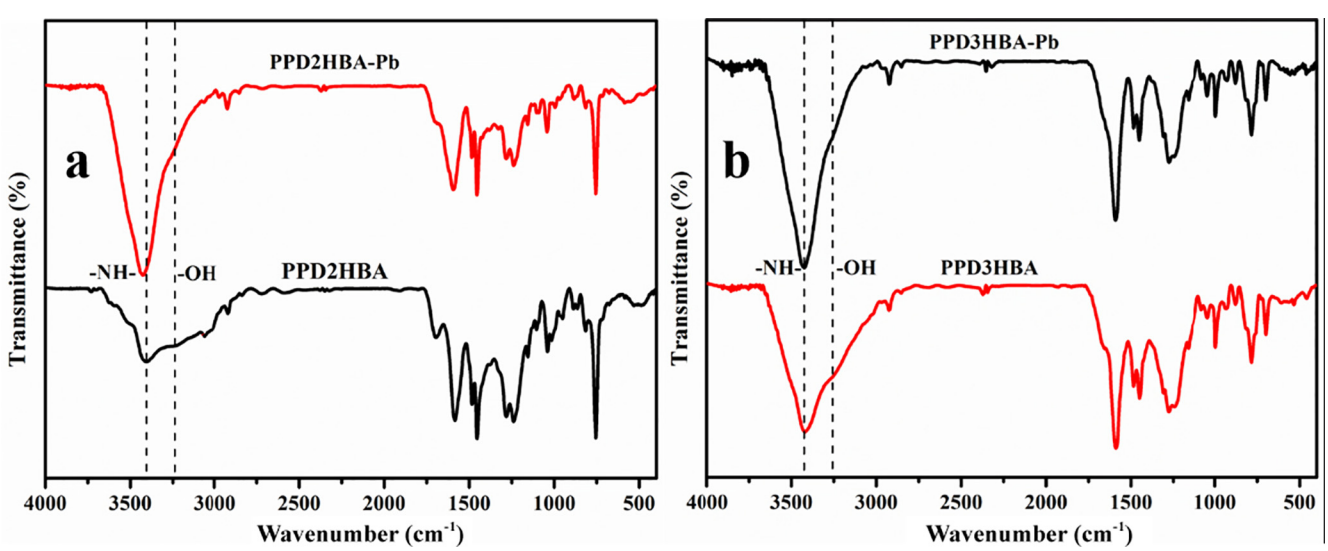

Fig. 10. FT-IR spectra of the adsorbents before and after adsorption: (a) PPD2HBA and PPD2HBA-Pb; (a) PPD3HBA and PPD3HBA-Pb.

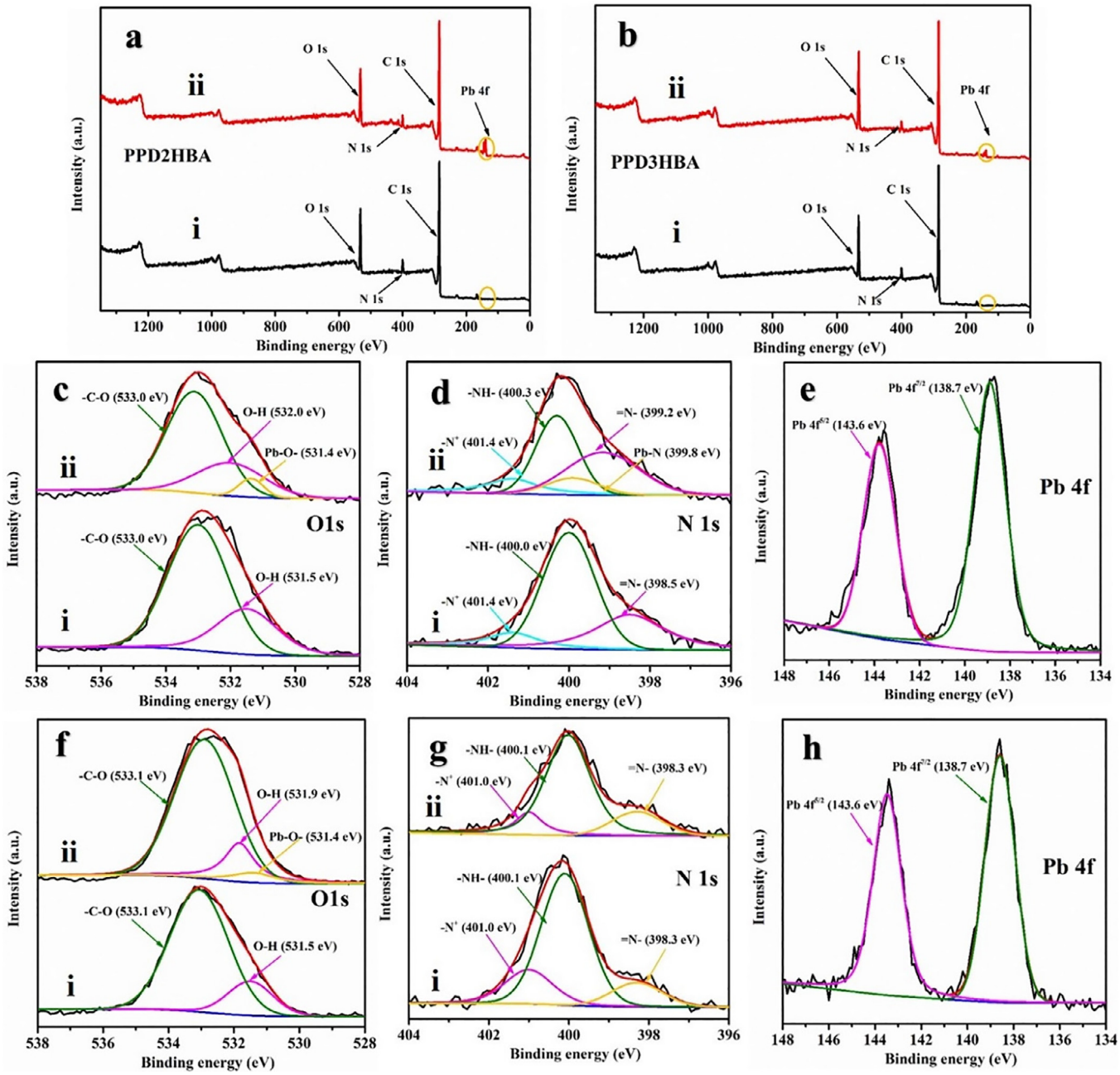

Fig. 11. Full scan survey XPS spectra: (a) PPD2HBA and (b) PPD3HBA, High resolution spectra of (c) O 1 s (d) N 1 s and (e) Pb 4f of PPD2HBA, (f) O 1 s (g) N 1 s and (h) Pb 4f of PPD3HBA (i) before and (ii) after Pb^{2+} adsorption.

respectively. Obviously, it can be seen that these selective coefficient values of PPD2HBA and PPD3HBA are greater than these of other common adsorbents, which indicate that PPD2HBA and PPD3HBA have relatively good adsorption selectivity to Pb^{2+} ions in complex solution containing many other metal ions.

3.3.2. *Effect of the steric hindrance on the selective adsorption of Pb^{2+}*

Heavy metal ions dissolve into solution in the form of hydrated ions, which have different hydrated ions radius [50]. Thus, the specific metal ions can be selectively adsorbed by the adsorbent which has be designed with suitable steric hindrance. In order to testify the influence of steric hindrance on the selective adsorption of Pb^{2+}, the substituent position of hydroxyl onto poly(pyrrole methane) is changed sequentially, which could be proved by ^{1}H NMR (Fig. S3), FT-IR (Fig. S4) and UV–Vis absorption (Fig. S5). Thus, PPD4HBA is synthesized and subsequently used to adsorb Pb^{2+} in the same condition. The chemical structures of the three poly(pyrrole methane)s are shown in Fig. 9, Observed from Table 6, the adsorption capacities of Pb^{2+} onto the three kinds of adsorbents are different. The adsorption capacity of Pb^{2+} onto PPD2HBA is higher than that of PPD3HBA and PPD4HBA, while the values of PPD3HBA and PPD4HBA are nearly identical. The chemical structures of the three adsorbents are almost similar except the substituent positions of hydroxyl groups. So the Pb^{2+} adsorption capacity maybe be intensively influenced by the steric hindrance, which are generated by the distinct substituent positions of hydroxyl groups. Similar phenomena of steric hindrance on the adsorption process have also been observed [51,52]. The results indicate that the size and shape of Pb^{2+} agree with PPD2HBA's steric hindrance more than that of PPD3HBA and PPD4HBA.

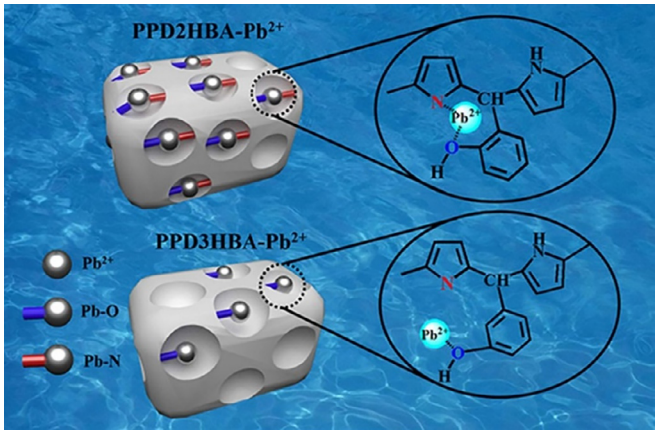

Fig. 12. The mechanism of the selective adsorption of Pb^{2+} onto the two adsorbents.

3.3.3. The plausible adsorption mechanism

FT-IR is used to analyze the change of the adsorbents before and after adsorption by identifying the main groups bonding with the Pb^{2+}, which could testify the steric hindrance effect in the adsorption process. As shown in Fig. 10a, the stretching vibrations of functional group (–NH-) in PPD2HBA form a peak at 3405 cm^{-1} which shifts to 3425 cm^{-1} after adsorbing Pb^{2+}. Meanwhile, the –OH peak of PPD2HBA shifts from 3217 cm^{-1} to 3251 cm^{-1}. The shift of the two peaks could be related to the combination between the two functional groups and Pb^{2+}. FTIR spectra of PPD3HBA before and after adsorption of Pb^{2+} are shown in Fig. 10b. It could be observed that only stretching vibrations of –OH shifted from 3224 to 3264 cm^{-1}, but the obvious change of –NH- don't occur at the same time. This phenomenon can indicate that the combination between PPD3HBA and Pb^{2+} ions only happy to –OH, not –NH-.

XPS technique is also employed to further investigate the mechanism for the adsorption of Pb^{2+} onto poly(pyrrole methane)s. The XPS spectra of the two adsorbents (PPD2HBA and PPD3HBA) before and after the adsorption of Pb^{2+} are showed in Fig. 11. After adsorbing Pb^{2+}, the new Pb peaks are observed in the survey spectra of two adsorbents (Fig. 11a and b). In Fig. 11e and h, the detail XPS spectra exhibit doublets characteristic of Pb 4f appeared at 138.7 eV and 143.6 eV for Pb $4f^{7/2}$ and Pb $4f^{5/2}$ after the adsorption of Pb^{2+}, respectively [53]. The result further confirms that the adsorption of Pb^{2+} onto adsorbents. Fig. 11c is the high resolution of O1s peak of PPD2HBA before and after Pb^{2+} adsorption. A dominant peak at 533.0 eV and a shoulder peak at 531.5 eV are appeared after curve fitting, which are assigned to the oxygen-containing functional groups, –C–O and O–H, respectively [54,55]. After the adsorption of Pb^{2+}, the shoulder peak representing O–H shift from 531.5 eV to 532.0 eV. A new peak at 531.4 eV is observed in Fig. 11c (ii), which is contributed to the oxygen atom in Pb-O-. It also could be found that the area of O–H peak is decreased. These results prove the strong interaction between Pb^{2+} and –OH, which could also be obtained in Fig. 11h, representing the adsorption of Pb^{2+} onto PPD3HBA. In Fig. 11d (i), the binding energy bands of PPD2HBA at 398.5, 400.0 and 401.4 eV are assigned to =N–, –NH– and $–N^{+}–$, respectively [56,57]. After the adsorption of Pb^{2+} onto PPD2HBA, the three energy bands (=N–, –NH– and $–N^{+}–$) appear at 399.2 400.3 and 401.4 eV, respectively, and a new peak at 399.8 eV is observed in Fig. 11d (ii). These results indicate the nitrogen atom in Pb-N– is formed. However, the three energy bands (=N–, –NH– and $–N^{+}–$) have no changed and no new peak appears before and after Pb^{2+} adsorption onto PPD3HBA (Fig. 11g). These results certify that Pb^{2+} have no coupling with the nitrogen-containing functional groups of PPD3HBA. Based on the above XPS results, it can be assumed that –OH and –NH– containing oxygen and nitrogen of PPD2HBA play important roles to bind with Pb^{2+}. Meanwhile, it is obvious that Pb^{2+} can only cooperated with –OH of PPD3HBA. The observation are consistent with the FT-IR results.

Based on the above results, the adsorption mechanism of heavy metal ions about the steric hindrance effect could been obtained in this study (Fig. 12). In the adsorption process, the functional groups (–OH and –NH–) in the as-prepared adsorbents could combine with Pb^{2+}. Because the hydrated ionic radius of Pb^{2+} matches well with the space size between –OH and –NH– in PPD2HBA molecules, they further form a stable chemical structure which results in the selective adsorption. Meanwhile, for the adsorption of Pb^{2+} onto PPD3HBA, the chemical bonds form between Pb^{2+} and –OH due to the greater space size of –OH and –NH– in PPD3HBA molecules, which leads to an unstable and weak selective adsorption process. Therefore, the adsorption capacity and selectivity of PPD2HBA for Pb^{2+} is higher than that of PPD3HBA.

4. Conclusion

In this study, the adsorption behaviors of PPD2HBA and PPD3HBA for Pb^{2+} are studied to research the relationship between the selective adsorption of metal ions and the steric hindrance. The characterization of FT-IR, ^{1}H NMR, UV–Vis and XPS testify the successful synthesis of PPD2HBA and PPD3HBA. The test of SEM, BET and Zeta potential reveal the different physicochemical properties of the as-prepared adsorbents. The maximum adsorption capacities of Pb^{2+} onto PPD2HBA and PPD3HBA are 41.35 and 32.10 $mg{\cdot}g^{-1}$ at pH 6.0 and 318 K, respectively, resulted from the steric hindrance of PPD2HBA and PPD3HBA. The adsorption site of PPD2HBA for Pb^{2+} matches better with the size and shape of hydrated Pb^{2+} than that of PPD3HBA, which are confirmed by the FT-IR and XPS spectra of the two absorbents before and after Pb^{2+} adsorption. Meanwhile, the effect of the co-existing metal ions on Pb^{2+} adsorption and the adsorption capacity of Pb^{2+} onto PPD4HBA also certify the effect of the HASB theory and the steric hindrance. Therefore, this work has a further implication for the development in new economically selective adsorbent which can selectively capture the heavy metal ions in wastewater.

Acknowledgements

The authors gratefully acknowledge the Shaanxi Key research and development projects, China (Grant No. 2017SF-386), the financial supports from the National Natural Science Foundation of China (Grant No.21307098 and 21507104) and the Fundamental Research Funds for the Central Universities of China.

Appendix A. Supplementary data

Supplementary data to this article can be found online at https://doi.org/10.1016/j.cej.2018.12.093.

References

[1] B. Liu, X. Lv, X. Meng, G. Yu, D. Wang, Removal of Pb(II) from aqueous solution using dithiocarbamate modified chitosan beads with Pb(II) as imprinted ions, Chem. Eng. J. 220 (2013) 412–419.
[2] X.S. Jing, F.Q. Liu, Y. Xin, P.P. Ling, L.J. Li, L. Chao, A.M. Li, Adsorption performances and mechanisms of the newly synthesized N, N′-di (carboxymethyl) dithiocarbamate chelating resin toward divalent heavy metal ions from aqueous media, J. Hazard. Mater. 167 (2009) 589–596.
[3] R.K. Sharma, A. Puri, Y. Monga, A. Adholeya, Acetoacetanilide-functionalized Fe_3O_4 nanoparticles for selective and cyclic removal of Pb^{2+} ions from different charged wastewaters, J. Mater. Chem. A 2 (2014) 12888–12898.
[4] H. Bessbousse, T. Rhlalou, J.F. Verchère, L. Lebrun, Removal of heavy metal ions from aqueous solutions by filtration with a novel complexing membrane containing poly(ethyleneimine) in a poly(vinyl alcohol) matrix, J. Membr. Sci. 307 (2008) 249–259.
[5] F. Ge, M.M. Li, H. Ye, B.X. Zhao, Effective removal of heavy metal ions Cd^{2+}, Zn^{2+}, Pb^{2+}, Cu^{2+} from aqueous solution by polymer-modified magnetic nanoparticles, J. Hazard. Mater. 211–212 (2012) 366–372.
[6] N. Wang, J. Feng, J. Chen, J. Wang, W. Yan, Adsorption mechanism of phosphate by polyaniline/TiO_2 composite from wastewater, Chem. Eng. J. 316 (2017) 33–40.

[7] F. Ji, C. Li, B. Tang, J. Xu, G. Lu, P. Liu, Preparation of cellulose acetate/zeolite composite fiber and its adsorption behavior for heavy metal ions in aqueous solution, Chem. Eng. J. 209 (2012) 325–333.
[8] X. Luo, J. Zeng, S. Liu, L. Zhang, An effective and recyclable adsorbent for the removal of heavy metal ions from aqueous system: magnetic chitosan/cellulose microspheres, Bioresour. Technol. 194 (2015) 403–406.
[9] D. Wu, L. Hu, Y. Wang, Q. Wei, L. Yan, T. Yan, Y. Li, B. Du, EDTA modified β-cyclodextrin/chitosan for rapid removal of Pb(II) and acid red from aqueous solution, J. Colloid Interface Sci. 523 (2018) 56–64.
[10] P. Daorattanachai, F. Unob, A. Imyim, Multi-element preconcentration of heavy metal ions from aqueous solution by APDC impregnated activated carbon, Talanta 67 (2005) 59–64.
[11] S.A. Idris, S.R. Harvey, L.T. Gibson, Selective extraction of mercury(II) from water samples using mercapto functionalised-MCM-41 and regeneration of the sorbent using microwave digestion, J. Hazard. Mater. 193 (2011) 171–176.
[12] A.Z.M. Badruddoza, Z.B.Z. Shawon, J.D.T. Wei, K. Hidajat, M.S. Uddin, Fe_3O_4/cyclodextrin polymer nanocomposites for selective heavy metals removal from industrial wastewater, Carbohydr. Polym. 91 (2013) 322–332.
[13] F. Wang, X. Lu, X.Y. Li, Selective removals of heavy metals (Pb(2+), Cu(2+), and Cd(2+)) from wastewater by gelation with alginate for effective metal recovery, J. Hazard. Mater. 308 (2016) 75–83.
[14] L. Cui, Y. Wang, L. Gao, L. Hu, L. Yan, Q. Wei, B. Du, EDTA functionalized magnetic graphene oxide for removal of Pb(II), Hg(II) and Cu(II) in water treatment: Adsorption mechanism and separation property, Chem. Eng. J. 281 (2015) 1–10.
[15] S. Sun, L. Wang, A. Wang, Adsorption properties of crosslinked carboxymethyl-chitosan resin with Pb(II) as template ions, J. Hazard. Mater. 136 (2006) 930–937.
[16] A.H. Chen, C.Y. Yang, C.Y. Chen, C.Y. Chen, C.W. Chen, The chemically crosslinked metal-complexed chitosans for comparative adsorptions of Cu(II), Zn(II), Ni(II) and Pb(II) ions in aqueous medium, J. Hazard. Mater. 163 (2009) 1068–1075.
[17] H. Ge, T. Hua, X. Chen, Selective adsorption of lead on grafted and crosslinked chitosan nanoparticles prepared by using Pb^{2+} as template, J. Hazard. Mater. 308 (2016) 225–232.
[18] C. Esen, M. Andac, N. Bereli, R. Say, E. Henden, A. Denizli, Highly selective ion-imprinted particles for solid-phase extraction of Pb^{2+} ions, Mater. Sci. Eng., C 29 (2009) 2464–2470.
[19] S. Luo, X.E. Liu, D. Wu, G. Shi, T. Mei, Tunable conversion from saturable absorption to reverse saturable absorption in poly (pyrrole methine) derivatives, J. Mater. Chem. C 2 (2014) 8850–8853.
[20] S.A. Jenekhe, A class of narrow-band-gap semiconducting polymers, Nature 322 (1986) 345–347.
[21] Y. Zou, D. Gendron, R. Neagu-Plesu, M. Leclerc, Synthesis and Characterization of New Low-Bandgap Diketopyrrolopyrrole-Based Copolymers, Macromolecules 42 (2009) 6361–6365.
[22] C.Y. Yu, C.P. Chen, S.H. Chan, G.W. Hwang, C. Ting, Thiophene/phenylene/thiophene-based low-bandgap conjugated polymers for efficient near-infrared photovoltaic applications, Chem. Mater. 21 (2009) 3262–3269.
[23] C. Yang, H.S. Song, D.B. Liu, Pure blue light-emitting fluorene-based conjugated polymer with excellent thermal, photophysical, and electroluminescent properties, J. Mater. Sci. 48 (2013) 6719–6727.
[24] B. Li, L. Ye, E. Peng, Z. Tan, Synthesis, conductivity and photophysical properties of soluble low bandgap poly{(3-butyryl)pyrrole-[2,5-diyl(p-hydroxybenzylidene)]}, Synth. Met. 202 (2015) 33–38.
[25] D.K. Singh, S. Mishra, Synthesis and characterization of UO_2^{2+}-ion imprinted polymer for selective extraction of UO_2^{2+}, Anal. Chim. Acta 644 (2009) 42–47.
[26] B. Li, M. Shi, D. Yan, M. Bai, Synthesis and photophysical characterization of MWCNTs/poly(pyrrolyl methine), Chem. Phys. Lett. 662 (2016) 280–285.
[27] S. Abdi, M. Nasiri, A. Mesbahi, M.H. Khani, Investigation of uranium (VI) adsorption by polypyrrole, J. Hazard. Mater. 332 (2017) 132–139.
[28] X. Guo, B. Du, Q. Wei, J. Yang, L. Hu, L. Yan, W. Xu, Synthesis of amino functionalized magnetic graphenes composite material and its application to remove Cr (VI), Pb(II), Hg(II), Cd(II) and Ni(II) from contaminated water, J. Hazard. Mater. 278 (2014) 211–220.
[29] S.D. Morales, E. Mijangos, S. Pullen, M. Gao, A. Orthaber, Functional small-molecules & polymers containing P[double bond, length as m-dash]C and As[double bond, length as m-dash]C bonds as hybrid π-conjugated materials, Chem. Commun. 53 (2017) 1120.
[30] F. Deng, L. Min, X. Luo, S. Wu, S. Luo, Visible-light photocatalytic degradation performances and thermal stability due to the synergetic effect of TiO_2 with conductive copolymers of polyaniline and polypyrrole, Nanoscale 5 (2013) 8703–8710.
[31] M. Bhaumik, R. Mccrindle, A. Maity, Efficient removal of Congo red from aqueous solutions by adsorption onto interconnected polypyrrole-polyaniline nanofibres, Chem. Eng. J. 228 (2013) 506–515.
[32] D. Dinda, S.K. Saha, Sulfuric acid doped poly diaminopyridine/graphene composite to remove high concentration of toxic Cr(VI), J. Hazard. Mater. 291 (2015) 93–101.
[33] X. Xin, Q. Wei, J. Yang, L. Yan, R. Feng, G. Chen, B. Du, H. Li, Highly efficient removal of heavy metal ions by amine-functionalized mesoporous Fe_3O_4 nanoparticles, Chem. Eng. J. 184 (2012) 132–140.
[34] Y.S. Ho, J.F. Porter, G. Mckay, Equilibrium isotherm studies for the sorption of divalent metal ions onto peat: copper, nickel and lead single component systems, Water, Air, Soil Pollut. 141 (2002) 1–33.
[35] M. Karthikeyan, K.K. Satheeshkumar, K.P. Elango, Removal of fluoride ions from aqueous solution by conducting polypyrrole, J. Hazard. Mater. 167 (2009) 300–305.
[36] P.F. Fulvio, M. Jaroniec, C. Liang, S. Dai, Polypyrrole-based nitrogen-doped carbon replicas of SBA-15 and SBA-16 containing magnetic nanoparticles, J. Phys. Chem. C 112 (2008) 13126–13133.
[37] M. Bhaumik, A. Maity, V.V. Srinivasu, M.S. Onyango, Removal of hexavalent chromium from aqueous solution using polypyrrole-polyaniline nanofibers, Chem. Eng. J. 181–182 (2012) 323–333.
[38] K.R. Hall, L.C. Eagleton, A. Acrivos, T. Vermeulen, A. Acrivos, T. Vermeulen, Pore and solid diffusion kinetics in fixed-bed adsorption under constant pattern conditions, Ind. Eng. Chem. Fundam. 5 (1966) 212–213.
[39] M.S. Sajab, C.H. Chia, S. Zakaria, S.M. Jani, M.K. Ayob, K.L. Chee, P.S. Khiew, W.S. Chiu, Citric acid modified kenaf core fibres for removal of methylene blue from aqueous solution, Bioresour. Technol. 102 (2011) 7237–7243.
[40] Y. Wang, L. Hu, G. Zhang, T. Yan, L. Yan, Q. Wei, B. Du, Removal of Pb(II) and methylene blue from aqueous solution by magnetic hydroxyapatite-immobilized oxidized multi-walled carbon nanotubes, J. Colloid Interface Sci. 494 (2017) 380–388.
[41] A. Chatterjee, T. Ebina, T. Iwasaki, F. Mizukami, Intermolecular reactivity study to scale adsorption property of para- and meta-substituted nitrobenzene over 2:1 dioctahedral smectite, J. Chem. Phys. 118 (2003) 10212–10220.
[42] B. Saville, The concept of hard and soft acids and bases as applied to multi-center chemical reactions, Angew. Chem., Int. Ed. 6 (2010) 928–939.
[43] B. Liu, C. Wei, X. Peng, Q. Cao, Q. Wang, D. Wang, X. Meng, G. Yu, Biosorption of lead from aqueous solutions by ion-imprinted tetraethylenepentamine modified chitosan beads, Int. J. Biol. Macromol. 86 (2016) 562–569.
[44] N. Wang, X. Xu, H. Li, L. Yuan, H. Yu, Enhanced Selective Adsorption of Pb (II) from Aqueous Solutions by One-Pot Synthesis of Xanthate-Modified Chitosan Sponge: Behaviors and Mechanisms, Ind. Eng. Chem. Res. 55 (2016) 12222–12231.
[45] M. Aliabadi, M. Irani, J. Ismaeili, H. Piri, M.J. Parnian, Electrospun nanofiber membrane of PEO/Chitosan for the adsorption of nickel, cadmium, lead and copper ions from aqueous solution, Chem. Eng. J. 220 (2013) 237–243.
[46] Y. Bulut, Z. Tez, Adsorption studies on ground shells of hazelnut and almond, J. Hazard. Mater. 149 (2007) 35–41.
[47] A.A. Taha, M.A. Shreadah, A.M. Ahmed, H.F. Heiba, Multi-component adsorption of Pb(II), Cd(II), and Ni(II) onto Egyptian Na-activated bentonite; equilibrium, kinetics, thermodynamics, and application for seawater desalination, J. Environ. Chem. Eng. 4 (2016) 1166–1180.
[48] M.E. Mahmoud, G.M. Nabil, S.M.E. Mahmoud, High performance nano-zirconium silicate adsorbent for efficient removal of copper (II), cadmium (II) and lead (II), J. Environ. Chem. Eng. 3 (2015) 1320–1328.
[49] W. Xu, W. Yang, W. Zhou, Selective solid-phase extraction of Pb(II) ions using an ion-imprinted functionalized sodium trititanate whisker adsorbent prepared by a surface-imprinting technique, Adsorpt. Sci. Technol. 28 (2010) 509–519.
[50] F. Fu, Q. Wang, Removal of heavy metal ions from wastewaters: a review, J. Environ. Manage. 92 (2011) 407–418.
[51] W. Liu, T. Wang, A.G. Borthwick, Y. Wang, X. Yin, X. Li, J. Ni, Adsorption of Pb^{2+}, Cd^{2+}, Cu^{2+} and Cr^{6+} onto titanate nanotubes: competition and effect of inorganic ions, Sci. Total Environ. 456–457 (2013) 171–180.
[52] X. Dong, C. Wang, H. Li, M. Wu, S. Liao, D. Zhang, B. Pan, The sorption of heavy metals on thermally treated sediments with high organic matter content, Bioresour. Technol. 160 (2014) 123–128.
[53] S. Pan, J. Li, G. Wan, C. Liu, W. Fan, L. Wang, Nanosized yolk-shell Fe_3O_4@$Zr(OH)_x$ spheres for efficient removal of Pb(II) from aqueous solution, J. Hazard. Mater. 309 (2016) 1–9.
[54] Y. Li, R. Zhao, Y. Pang, X. Qiu, D. Yang, Microwave-assisted synthesis of high carboxyl content of lignin for enhancing adsorption of lead, Colloids Surf A 553 (2018) 187–194.
[55] Z. Chang, Z. Yu, G. Zeng, B. Huang, H. Dong, J. Huang, Z. Yang, J. Wei, H. Liang, Z. Qi, Phase transformation of crystalline iron oxides and their adsorption abilities for Pb and Cd, Chem. Eng. J. 284 (2016) 247–259.
[56] W. Hou, X. Yuan, W. Yan, X. Chen, L. Leng, W. Hui, L. Hui, G. Zeng, Facile synthesis of polypyrrole decorated reduced graphene oxide–Fe_3O_4 magnetic composites and its application for the Cr(VI) removal, Chem. Eng. J. 262 (2015) 597–606.
[57] T. Liu, X. Han, Y. Wang, L. Yan, B. Du, Q. Wei, D. Wei, Magnetic chitosan/anaerobic granular sludge composite: synthesis, characterization and application in heavy metal ions removal, J. Colloid Interface Sci. 508 (2017) 405–414.